# FINITE ELEMENT METHOD ANALYSIS OF VARIABLE INDUCTOR BASED DC-DC CONVERTERS FOR ELECTRIC VEHICLES

**Mebrahtom Beraki[1], João P. Trovão[1,3,4], A. S. Mohammadi[1], M. Dubois[1], M. Perdigão[2,3]**

[1]e-TESC Laboratory, Dept. Electrical & Computer Engineering, University of Sherbrooke, Quebec, Canada

[2]Instituto de Telecomunicações, DEEC, University of Coimbra, Polo II, 3030-290, Coimbra, Portugal

[3]Polytechnic Institute of Coimbra, IPC-ISEC, DEE, 3030-199, Coimbra, Portugal

[4]INESC Coimbra, DEEC, University of Coimbra, Polo II, 3030-290, Coimbra, Portugal

{Mebrahtom.Beraki, Joao.Trovao, Ahmad.Shah.Mohammadi, Maxime.Dubois}@USherbrooke.ca and perdigao@isec.pt

**Abstract -** This paper presents the Finite Element Method (FEM) simulation and analysis of a toroidal Variable Inductor (VI). In systems where there is high dynamics in power demand like Electric Vehicles (EVs), the power inductor is pushed to work in the saturation region several times. In order to overcome this challenge, a current controlled VI is used for the purpose of controlling the saturation level of a power inductor in a bidirectional DC-DC converter for EV applications. Simultaneously, there is an attempt to reduce the size and weight of the power inductors in power converters by using this technology. The studied VI is built with two toroidal cores and is composed of multiple windings, which makes it to have a complex geometry. In addition to its complex geometry, its magnetic properties and non-linear behavior complicate its modeling, analysis and understanding of its behavior. To simplify this and for an easier understanding of its concepts, a simplified mathematical representation of the operation of this device is illustrated and MagNet Simulation software is used for its modeling and analysis.

**Keywords** – Magnetic Device, DC-DC converter, MagNet Simulation, Saturation, Linkage flux

## 1. INTRODUCTION

Power electronics converters are key enabling technologies in converting and adapting power levels in several practical applications [1]. In fact, their size, efficiency and power density are fundamental requirements that need an immediate attention both at the design and implementation stages. The magnetic components (particularly the power inductor) are among the heaviest and largest components in power electronics converters. This is mainly due to the magnetic core and a number of conductors wound around the magnetic material [2]. Furthermore, this component plays a significant role in the operation of power electronic converters in several applications, for which the design, sizing and selection are very critical [3].

Size reduction and performance enhancement of this particular component can result in a remarkable reduction in the size and weight of power electronic converters. In most cases, the sizing and selection of the power inductors is performed based on the peak to peak current ripple and the rated current [4]. Nonetheless, in the case of power electronic converters for EVs, the power inductor may be forced to operate with currents much higher than the nominal rating and peak to peak ripple. This leads to the saturation of the magnetic core resulting in more losses due to higher current ripples.

One way to avoid the saturation of the power inductor in EV converters is to select this component in accordance to the high transient currents. Nonetheless, this will increase the size of the drivetrain of EVs and it is also inefficient. To address the aforementioned issues, the concept of VI, proposed in earlier work, is studied in order to explore its viability for EV applications.

Several ways of reducing the size of this component such as servo-systems [5] and moving air gap [6] have been used to mechanically change the effective inductance of power inductors. Nonetheless, these approaches are demanding and they fail to provide wide range of flexibility in adjusting the effective inductance of power inductors [7]. Consequently, the current controlled VIs are developed and proved to be promising for several applications [8]. These devices are composed of multiple windings, where there is multiple interaction of magnetic and electrical parameters. Furthermore, they have a complex geometry, diverse magnetic properties, and non-linear behavior. This makes them more complex to model, analyze and understand.

The FEM analysis and the SPICE modelling are the two methods commonly used for the analysis and

understanding of the complex magnetic phenomena of these devices [9]. The first has better accuracy but requires considerable time in modelling and simulation of such magnetic devices. It should also be noted that such simulation method provides the various parameters that can be very useful for understanding such kind of devices. The SPICE modelling provides a reasonable result with less accuracy compared to FEM analysis and faster simulation results can be obtained. Considering its accuracy and physical significance, the FEM analysis is used to model, analyze and study the VI topology.

The 2D and 3D FEM simulations of a toroidal inductor for studying the saturation characteristics and power losses of a power inductor is presented in [10]. Similarly, the non-linear FEM simulation of a power inductor is illustrated in [11]. Furthermore, other authors have studied the FEM simulation of coupled inductors [12], [13]. The FEM simulation of Double E core VI is also provided in [5].

In this paper, a double toroidal based VI is studied and modelled in *MagNet* software. Compared to the aforementioned studies, this work provides the analysis of the VI concept, its characterization as a function of two currents (the main winding current ($i_s$) and the control winding current ($i_b$). It provides the linkage flux ($\lambda$)-$i_s$ curves, and the differential inductances as a function of the control current. Furthermore, the principle of operation of this device is illustrated with the flux distribution diagrams for various current levels. The salient contributions of this work are on the modelling, analysis and simulation of a toroidal core based on VIs for applications with dynamic and wide range of load variations such as EVs.

## 2. SYSTEM DESCRIPTION

The studied power inductor is used in the bidirectional converter for EV applications, shown in Fig.1. The detailed modeling of the overall system in relation to the control and the significance of VI in ripple control for such kind of converters has been studied in [14]. As it can be clearly shown in Fig. 1, the conventional inductor is replaced by a VI. The VI is composed of two groups of windings, the main windings and the control windings. The main windings carry the main current and the control windings are used to control the saturation level of the magnetic core by canceling part of the magnetic flux in the main winding, using a small control current. The main windings of each core are connected in series with one another. Similarly, the auxiliary windings are also connected in series, but the windings are wound in such a way that the net reflected voltage in each winding is cancelled. As revealed in Fig.2, the VI is realized by two magnetically decoupled magnetic cores. The use of two decoupled magnetic cores helps in reducing the magnetic coupling between the same windings and reduce the voltage reflection effects. Each one of the two cores (core 1 and core 2) is made up by stacking of two smaller cores made of the same material. The specifications and dimensions of each smaller core is shown in Table I. The main winding flux and control winding flux oppose one another in core 1, but add up in core 2. This results in the partial saturation operation of the main winding leading to improving the current handling of the main winding before reaching its saturation limit.

The number of turns in the auxiliary windings are made much higher than that of the main winding; in order to have smaller control currents in the auxiliary winding. Having higher number of turns helps in increasing the control flux at smaller currents, which makes the control winding ohmic losses smaller. It is important to note that having higher number of turns, with smaller cross sectional area, increases the ohmic resistance of the control winding. Nonetheless, the impact of control current is more significant than the impact of resistance.

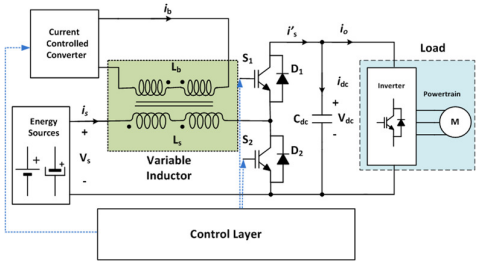


Fig. 1. VI in a bidirectional converter

**Table I: Specifications the VI prototype**

| Ferrite core Toroid R 102 × 65.8 × 15.0 (mm) with Epoxy coating | |
|---|---|
| Core material | N87 from EPOCS |
| Main winding wire gauge | 4.17mm$^2$ |
| Bias winding gauge | 0.65mm$^2$ |
| Main winding number of turns | 28 |
| Auxiliary winding number of turns | 360 |
| Total Volume of VI | 0.273dm$^3$ |

Before introducing the FEM simulation and results analysis of the VI, it is vital to reveal the analytical principles of operation and mathematical laws which govern its operation. Hence, a tacit review of the fundamental concepts is illustrated.

The operation of the VI topology shown in Fig.2 can be illustrated with the Ampere's law. The flux intensity as a function of both the main winding and auxiliary winding parameters such as the number of windings and currents of each winding can be written as:

$$H_1 = \frac{N_m i_s - N_c i_b}{2l} \quad (1)$$

$$H_2 = \frac{N_m i_s + N_c i_b}{2l} \quad (2)$$

where $H_1$, $H_2$, $N_m$, $i_s$ , $N_c$, $i_b$ and $l$ are the magnetic field intensity of core 1 and core 2, the total main winding number of turns, the main winding current, the auxiliary winding total number of turns, the

auxiliary winding current and the mean length of the magnetic core in respective order.

In magnetic materials, the magnetic flux density, $B$, and the magnetic field intensity, $H$, are related by the permeability of the material, $\mu$, as:

$$B = \mu H \qquad (3)$$

The total flux of a magnetic coil multiplied by the number of turns gives the flux linkage ($\lambda$).

$$\lambda = N_m \oint BdA = N_m BA \qquad (4)$$

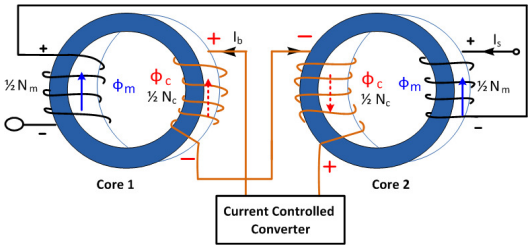


Fig. 2. Schematic diagram of the selected VI

Replacing $B$ in (4) by (3) the flux linkage ($\lambda$) can be written as:

$$\lambda = N_m \mu H A \qquad (5)$$

It should be noted that both the main winding coils are electrically connected but they are magnetically isolated. The magnetic isolation of the two windings helps in reducing the magnetic interaction between the two windings.

Rewriting the magnetic flux linkage in terms of the main current and auxiliary current, the flux linkage in core 1 and core 2 can be rewritten as:

$$\lambda_1 = N_m \mu A \left(\frac{N_m i_s - N_c i_b}{2l}\right) \qquad (6)$$

$$\lambda_2 = N_m \mu A \left(\frac{N_m i_s + N_c i_b}{2l}\right) \qquad (7)$$

From the flux linkages in (6) and (7), the inductances $L_1$ and $L_2$ of each the main windings can be calculated as shown in (7) and (8).

$$L_1 = \frac{\lambda_1}{i_s} \qquad (8)$$

$$L_2 = \frac{\lambda_2}{i_s} \qquad (9)$$

As the two windings are electrically connected the total inductance of the main winding will be the sum of the two inductances calculated (8) and (9). The differential inductance ($L_{dif}$) can also be calculated as:

$$L_d = \frac{d\lambda}{di_s} \qquad (10)$$

From (6) - (9) it can be shown that the inductance depends on the flux linkage, which is also a function of both the main winding and the auxiliary winding currents. Hence, the saturation level and the effective inductance can be adjusted by changing the current in the auxiliary winding. The above equations reveal that both the inductance and the differential inductance depend upon the geometry of the core material, permeability, and the Magnetomotive Force (MMF). By using an auxiliary winding, the net MMF of a magnetic material can be regulated by changing the permeability of the material as a function of the two currents hence, its saturation can be regulated.

## 3. Finite Element Method Simulation and Analysis of the Selected VI

In the modelling of the studied VI configuration, the model of the VI is built in the *MagNet infolytica* software. The FEM simulation of the studied VI is composed of the modelling, the simulation and the post processing phases. In the first phase, the geometrical model is created and the materials for each section are selected.

In this study, the selected material is N87 from EPOCS [15] with the dimensions shown in Table I and its *B-H* characteristics curve is revealed in Fig.4.

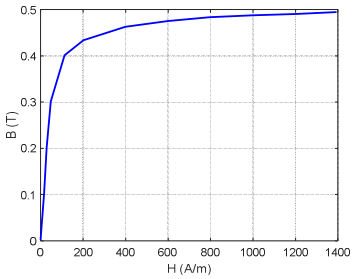


Fig. 3. Selected Material B-H Curve

Following the modelling phase, the model is simulated in order to solve Maxwell's equations to determine the magnetic fields distribution, energy, linkage flux and other important parameters. 3D transient simulation is used.

In the post simulation processing phase, where there are different options to view the magnetic fields distribution in the model. The distribution of several quantities can be viewed both as counter plot, shaded plot and arrow plots. Furthermore, several quantities can be extracted in the global results window. In this study, the parameters of interest are extracted and analyzed. Both the stored energy and linkage flux are vital quantities in order to study the variations of inductance as a function of both the main winding and control winding currents. From the stored energy, the main winding inductance can be estimated as:

$$L = \frac{2E}{i_s^2} \qquad (11)$$

where $E$ is stored energy in the power inductor and $i_s$ is the main winding current across the inductor.

Furthermore, the inductance can also be calculated from the flux linkage using (8) and (9). The energy obtained from the *FEM* simulation is the total energy of the complete system including the boundary where the problem is solved. Estimating the inductance

using this approach can result in slight deviations. The linkage inductance approach provides better results and accuracy [16]; hence it is used in the inductance characterization of the VI using the formulas presented in (7) - (8).

In order to study the modelled VI topology, the linear region and the saturation region operation are studied by changing the main winding current using transient analysis. Also, the inductance value of each operating point is obtained from the flux linkage simulation results using the formulas presented in (8) and (9).

After studying its characteristics of the VI with no control current in the auxiliary winding, different control currents are applied to the auxiliary winding. in order to study the impact of the control current on the magnetic properties of the magnetic material. Then, the linkage flux is used for the characterization of the VI. Fig. 4 reveals the linkage flux versus main winding current for different control currents in the auxiliary winding. It has to be noted that the $\lambda$-$i_s$ curves are for core 1. As core 2 is saturated due to the addition of dc flux, the $\lambda$-$i_s$ curves of it are not included due to space limitations. The $\lambda$-$i_s$ curves are obtained by applying a ramp current in the main winding and the control current is varied. With the increase of current in the auxiliary winding, it can be shown that the saturation of the power inductor is delayed, i.e. the core starts to saturate at higher main winding currents as we increase the control current. This is mainly due to the partial cancelation of magnetic flux, which reduces the saturation effect of the magnetic core. Furthermore, it can also be shown that, if the main winding current is small, higher control currents can lead to the saturation of the magnetic core in the opposite direction. For smaller currents in the main winding smaller auxiliary winding currents are enough to cancel out the fluxes in order to enable partial saturation operation. Nonetheless, for currents much larger than the saturation current of the main winding, it is necessary that the MMF of the auxiliary winding is sufficient to reduce part of the main MMF, which can lead to the saturation of the magnetic core. Therefore, by applying appropriate control currents, the current handling capability of the power inductor can be regulated.

The aforementioned concepts can be summarized with the differential inductance. Considering two operating currents (13.5 A and 14 A) in each of curves shown in Fig.4. The values of flux linkages for each curve shown in the selected points of operation are shown in Table II. From these information, the differential inductance of each curve is calculated using (11).

$$L_d = \frac{\lambda_{p2} - \lambda_{p1}}{i_{s2} - i_{s1}} \qquad (11)$$

In the first blue curve, there is no control current applied, as a result there is very small variation both in the change of linkage flux and the differential inductance between the two selected operating points.

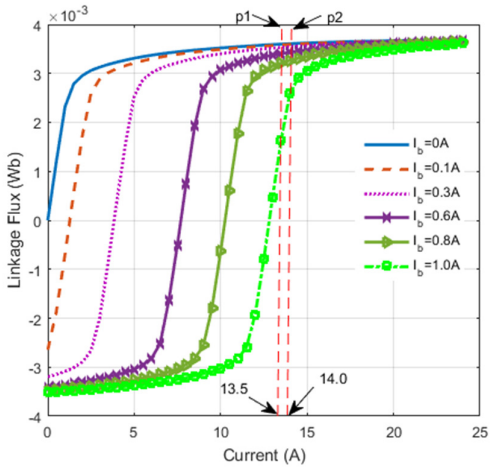


Fig. 4. Linkage flux as a function of the main winding current for different control currents (core 1)

This indicates that the magnetic core is saturated in the selected points of operation. Nonetheless, as we increase the control current, it can be shown from Table II, both the change in linkage flux and the differential inductance tend to increase. In the curve with a control current of 1 A, the differential inductance is more than 100 times higher than the differential inductance of the curve with no control current in the auxiliary winding. This is mainly due to the partial cancelation of the main winding flux which results in the enhancement of the saturation level of by delaying the saturation of the magnetic core.

Table II: Parameters for calculating the differential inductance

| $i_b(A)$ | $\lambda_{p1}(Wb)$ $i_s$=13.5A | $\lambda_{p2}(Wb)$ $i_s$=14A | $\Delta\lambda(\mu Wb)$ | $L_d(\mu H)$ |
|---|---|---|---|---|
| 0 | 0.003598 | 0.003607 | 8.60 | 17.2 |
| 0.1 | 0.003582 | 0.003591 | 9.14 | 18.3 |
| 0.3 | 0.003531 | 0.003546 | 14.9 | 29.9 |
| 0.6 | 0.003403 | 0.003431 | 27.3 | 54.7 |
| 0.8 | 0.003212 | 0.003265 | 53.1 | 106 |
| 1.0 | 0.001632 | 0.002588 | 956 | 1910 |

All in all, from the last two columns of Table II, it can be inferred that, this approach can be very helpful in increasing the saturation current limit of power inductors, which is very suitable for EV applications to overcome the larger inductors demand due to saturation constraint.

In the simulations, the control current is applied for all levels of the main winding current in order to understand its impact on the operation of the power inductor. It should be also noted that, for small main

winding currents, applying larger control currents can lead to the saturation of the magnetic core in the opposite direction as shown in Fig.4. This information could be very helpful in the development of control strategy of VI-based converters and design of VI for traction applications. In the practical implementation of this device, the control winding should be idle for currents less than the saturation current. For currents greater than the control, winding should be activated to regulate the effective inductance of the magnetic core.

Fig. 5 shows the impact of the control current in the losses of the power inductor. Two operating currents ($i_s$=12 A and $i_s$=16 A) are selected and the control current is varied to study its impact on the global losses of the power inductor. The core losses are determined from the simulation using Steinmetz formula presented in [17].

In both cases, the copper and core losses are shown to fall as a function of the control current. With a proper control current, the main winding losses can be reduced by 6 % for 12 A and 4 % for 16 A with the help of VI by regulating the magnetic flux.

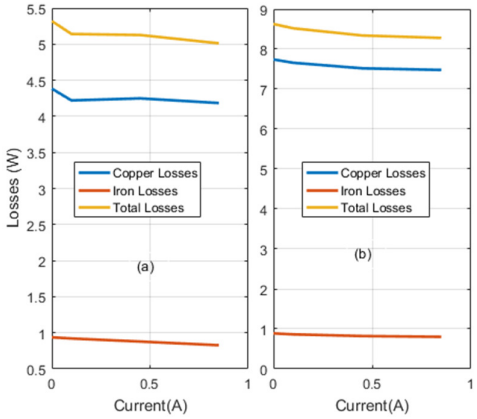


Fig. 5. Losses as a function of the control current for both cores and considering: (a) $i_s$=12 A; (b) $i_s$=16 A

The *MagNe*t simulation software results shown in Fig. 6 illustrate the distribution of magnetic flux density for different main and control winding currents. The first two figures (a) and (b) show that the magnetic cores are operating in the linear region and this is clearly revealed from the flux distribution in the magnetic cores. Further increasing the main winding current leads to the saturation of the magnetic cores. For the cases of (c) and (e), as there is no control current applied, both cores are shown to be saturated. For a main current of 19 A, the magnetic cores are deeply saturated, hence, higher control current is needed in order to enable it to operate in the partial saturation mode. However, in (d) and (f) a control current is applied, and it can be shown that the first cores are operating in the linear region and the second cores are forced to operate in saturation. This leads to the partial saturation application and can be used to control the inductance of power inductors. It is important to note that this operation helps in reducing the voltage reflection between the two groups of coils resulting in reducing the losses in the magnetic cores.

In the linear region, there is higher flux variation, but in the saturation region, the variation of flux is minimal due to the alignment of the magnetic dipoles in the direction of the applied field. From Fig.6, it can be shown that increasing the control current can significantly enhance current handling capability of power inductors and delays the saturation of one of the magnetic cores. But higher currents in the auxiliary winding can contribute to the increase of the global losses. Therefore, the auxiliary winding should be designed to handle smaller currents and the control current needs to be kept smaller in proportion to the main winding current.

(a) $i_s$=1.0 A, $i_b$=0 A  b) $i_s$=2.0 A, $i_b$=0 A

(c) $i_s$=6.5 A, $i_b$=0 A  (d) $i_s$=14.5 A, $i_b$=1.0 A

(e) $i_s$=19.0 A, $i_b$=0 A  (f) $i_s$=19.0 A, $i_b$=1.45 A

Fig. 6. Flux distributions without and with control current in the auxiliary winding

Furthermore, the inductance curve as a function of main winding current of the simulated VI-prototype and the experimental studies of the same VI studied in [14] are presented in Fig. 7.

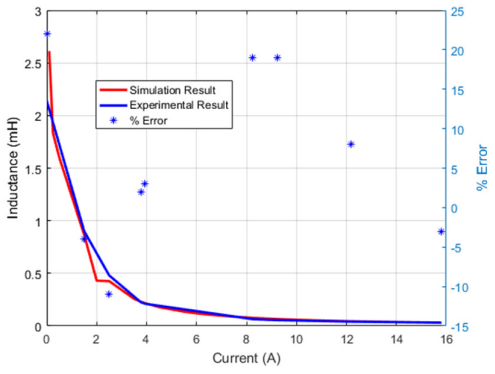


Fig. 7. Large signal characterization of both simulation and experimental results

The simulation inductance results are obtained using (8) and (9) and the experimental values of inductance are calculated using the following formula:

$$L = \frac{DV_s}{f_{sw}\Delta i_L} \qquad (13)$$

where $D$ is the duty cycle, $V_s$ is the source voltage, $f_{sw}$ is the switching frequency (Hz) and $\Delta i_L$ is the peak to peak inductor current ripple. Except at lower currents, the inductance obtained form the simualtion and experimental results match to each other with an averge error of 6 %, which validates the accuracy of the FEM model of the VI prototype.

## 4. CONCLUSION

This paper presents the FEM analysis of a toroidal VI prototype with a particular emphasis on studying its feasibility for applications with dynamic and wide load variations. The mathematical expressions that illustrate the operation of the VI are presented. The 3D FEM simulation is used to model the VI under study. From the simulations, the flux distribution, $\lambda - I_s$ characterization curve, the differential inductance and the losses trends are analyzed. Furthermore, the inductance characteristics of the VI is obtained from simulations and the results are in agreement with the experimental results with an average error of 6%. From the $\lambda - I_s$ characterization curve, it can be deduced that by applying small control current in the auxiliary winding of the VI, the current handling capability of the magnetic core is enhanced. Subsequently, the saturation of the magnetic core is delayed. With the help of these results, the future trends will focus on development of control strategies and design of the VI for traction applications.

## ACKNOWLEDGEMENTS

This work was supported in part by the Canada Research Chairs Program and by the Portuguese Foundation for Science and Technology (FCT) under project grant UID/MULTI/00308/2013.

## REFERENCES

[1] J. D. V. Wyk and F. C. Lee, "On a Future for Power Electronics," *IEEE Journal of Emerging and Selected Topics in Power Electronics,* vol. 1, no.2, pp. 59-72, 2013.

[2] Z. Dang and J. A. A. Qahouq, "Evaluation of High-Current Toroid Power Inductor With NdFeB Magnet for DC-DC Power Converters," *IEEE Transactions on Industrial Electronics,* vol. 62, no.11, pp. 6868-6876, 2015.

[3] Z. Dang and J. A. A. Qahouq, "Modeling and design guidelines of high density power inductor for battery power unit," in *2016 IEEE Applied Power Electronics Conference and Exposition (APEC)*, 2016, pp. 2114-2121.

[4] M. S. Perdigão, J. P. F. Trovão, J. M. Alonso, and E. S. Saraiva, "Large-Signal Characterization of Power Inductors in EV Bidirectional DC–DC Converters Focused on Core Size Optimization," *IEEE Transactions on Industrial Electronics,* vol. 62, no.5, pp. 3042-3051, 2015.

[5] Y. Bi and D. C. Jiles, "Finite element modeling of an electrically variable inductor," *Magnetics, IEEE Transactions on,* vol. 35, no.5, pp. 3517-3519, 1999.

[6] W. G. Hurley and W. H. Wölfle, *Transformers and inductors for power electronics: theory, design and applications*: John Wiley & Sons, 2013.

[7] Y. Bi and D. Jiles, "Finite element modeling of an electrically variable inductor," *IEEE transactions on magnetics,* vol. 35, no.5, pp. 3517-3519, 1999.

[8] M. S. Perdigão, M. Menke, A. Seidel, R. A. Pinto, and J. M. Alonso, "A review on variable inductors and variable transformers: Applications to lighting drivers," *IEEE Transactions on Industry Applications,* vol. 52, no.1, pp. 531-547, 2016.

[9] J. M. Alonso, G. Martinez, M. Perdigão, M. Cosetin, and R. N. d. Prado, "Modeling magnetic devices using SPICE: Application to variable inductors," in *2016 IEEE Applied Power Electronics Conference and Exposition (APEC)*, 2016, pp. 1115-1122.

[10] R. A. Salas and J. Pleite, "Simulation of Waveforms of a Ferrite Inductor with Saturation and Power Losses," *Materials,* vol. 7, no.3, pp. 1850-1865, 2014.

[11] R. A. Salas and J. Pleite, "Simulation of nonsinusoidal waveforms of ferrite inductors with saturation and power losses using electromagnetic modeling in 2D," in *Electromagnetics in Advanced Applications (ICEAA), 2013 International Conference on*, 2013, pp. 45-48.

[12] Y. Su, Q. Li, and F. C. Lee, "FEA modeling of the low profile coupled inductor with non-uniform flux distribution," in *Applied Power Electronics Conference and Exposition (APEC), 2013 Twenty-Eighth Annual IEEE*, 2013, pp. 2416-2423.

[13] A. M. Knight and J. Salmon, "3D finite element analysis of coupled inductors for multilevel inverter output," in *Electromagnetic Field Computation (CEFC), 2010 14th Biennial IEEE Conference on*, 2010, pp. 1-1.

[14] M. Beraki, J. P. Trovao, M. Perdigao, and F. Machado, "Bidirectional DC-DC Converter Using Variable Inductor Concept for Electric Vehicle Applications," in *Vehicle Power and Propulsion Conference (VPPC), 2016 IEEE*, 2016, pp. 1-6.

[15] A. EPCOS, "Ferrites and accessories-SIFERRIT material N87," *Data Sheet, September,* 2006.

[16] R. Escarela-Perez, E. Campero-Littlewood, M. A. Arjona-Lopez, and A. Laureano-Cruces, "Comparison of two techniques for two-dimensional finite-element inductance computation of electrical machines," *IEE Proceedings - Electric Power Applications,* vol. 152, no.4, pp. 855-861, 2005.

[17] D. W. Kim, H. Cha, S. H. Lee, and D. H. Kim, "Characteristic of a Variable Inductor Using Magnetorheological Fluid for Efficient Power Conversion," *IEEE Transactions on Magnetics,* vol. 49, no.5, pp. 1901-1904, 2013.